Breakthrough in Understanding Radiation Growth of Zirconium

Stanislav I. Golubov[1*], Alexander V. Barashev[1,2], Roger E. Stoller[1], and Bachu N. Singh[3]

[1]*Materials Science and Technology Division, ORNL, Oak Ridge, TN 37831- 6138, USA, golubovsi@ornl.gov, 1 865 5764920*
[2]*Center for Materials Processing, Department of Materials Science and Engineering, University of Tennessee, East Stadium Hall, Knoxville, TN 37996-0750, USA*
[3]*Materials Research Department, Risø National Laboratory, Technical University of Denmark, DK-4000 Roskilde, Denmark*

ABSTRACT

Efforts of many scientists for more than a half of a century have resulted in substantial understanding of the response of Zr-based materials to irradiation. However, the models of radiation growth proposed to date have not played decisive role in creating radiation-resistant materials and cannot predict strain rates at high irradiation doses. The main reason for this is the common assumption that, regardless of the incident particle mass and energy, the primary damage consists of single vacancies and self-interstitial atoms (SIAs), both diffusing three-dimensionally. So, the models ignore the distinguishing features of the damage production in displacement cascades during fast-particle, e.g. neutron, irradiation; namely, the intra-cascade clustering of vacancies and SIAs, and one-dimensional diffusion of SIA clusters. Over the last about twenty years, the Production Bias Model (PBM) has been developed, which accounts for these features and explains many observations in cubic crystals. The cascades in hcp crystals are found to be similar to those in cubic crystals; hence one can expect that the PBM will provide a realistic framework for the hcp metals as well. It is shown in this paper that it reproduces all the growth stages observed in annealed materials under neutron irradiation, such as the high strain rate at low, strain saturation at intermediate and breakaway growth at relatively high doses. It accounts for the striking observations of negative strains in prismatic directions and co-existence of vacancy- and interstitial-type prismatic loops, which have never been explained before. It reveals the role of cold work in the radiation growth behavior and the reasons for the alignment of basal vacancy-type loops along the basal planes. The critical parameters determining the high-dose behavior are revealed and the maximum growth rate is estimated.

*Key words***:** neutron irradiation, zirconium, radiation growth, theory

PACS codes: 61.80.Az.; 61.80.Hg., 61.82.Bg.

*Corresponding author. E-mail: golubovsi@ornl.gov.

1. Introduction

The radiation growth (RG) of Zr-based materials is one of the main concerns for the safe operation of thermal nuclear reactors, such as PWA and BWA. Experiments have demonstrated that deformation of these alloys at temperatures below ~300ºC is driven by the evolution of dislocation structure, which includes nucleation and growth of dislocation loops on both the prismatic and basal planes. The growth strain in *c* direction is always negative, and the basal-plane loops are always of the vacancy type. The strains in prismatic directions are positive in the majority of cases, but may also be negative. Another striking observation is that the prismatic loops of both vacancy and interstitial type may be formed at the same time.

It is commonly accepted that the RG occurs due to asymmetry of the capture efficiencies of *a* and *c* dislocations and dislocation loops for single vacancy and interstitial atoms. However, the conventional concept of dislocation bias suggests that, in this case, the strains must have opposite signs to those generally observed, i.e. positive/expansion in *c* and negative /contraction in *a* directions. This is because the Burgers vector of *c* dislocations is larger than that of *a* dislocations, which creates larger bias of *c* dislocations to self-interstitial atoms (SIAs). Several models have been proposed to resolve this contradiction since the first model by Buckley [1] ~50 years ago (see, e.g. [2] for a review), all based on the dislocation bias approach, but none has resolved the issue.

A qualitatively new step in understanding the RG phenomenon was made by Woo and Gösele [3, 4] by introducing anisotropic diffusion of SIAs on the hcp lattice. In the diffusion anisotropy difference (DAD) model [4], it was suggested that the vacancy diffusion is isotropic, whereas the SIAs migrate preferentially along the basal planes. This allowed explaining the contraction of *c* axes and the crucial role of *c* loops in developing breakaway stage in annealed Zr crystals.

Nevertheless, the DAD model does not describe correctly the RG in neutron-irradiated materials. This is because it assumes that the primary damage consists of point defects, i.e. single vacancies and SIAs, only. Experiments (see e.g. [5]) and molecular dynamics (MD) simulations (see, e.g. a recent review [6]) have shown that under neutron irradiation a large, ~20-50%, fraction of the defects form clusters. The SIA clusters migrate one-dimensionally (1-D), which results in the mixture of the second (for the point defects) and third (for the SIA clusters) order reaction kinetics in neutron-irradiated solids, rather than just second order, as in the DAD model. Holt and Woo [7] generalized the DAD model by accounting for the cascade production of SIA clusters, but assumed the clusters to be immobile, which was wrong. In fact, the MD simulations show that in all crystals including Zr [6,8,9] the SIA clusters are highly mobile, diffusing 1-D along close-packed directions. The authors of [7] made another assumption that "*…the higher reaction cross section with the primary clusters of the a-dislocations than of c-component dislocations, due to the higher mobility, by glide, of the former"*, which is unphysical, since there is no reason for dislocation glide without external stress. In the calculations presented in [7] the DAD bias factor was taken to be equal to 200%, which requires high anisotropy of single SIA diffusion, $D_a / D_c \approx 10^2$, which is not supported by *ab initio* calculations [10,11].

One more paper devoted to RG in Zr was published by Christien and Barbu [8], which, however, did not provide any new insight into the RG. The description of the breakaway stage in [8] is the

same as in the DAD model. The only innovation is the assumption that the RG strain at low doses is due to accumulation of single vacancies. The vacancy concentration required to reproduce observations is ~10^{-4}, i.e. close to the thermal-equilibrium value at the melting temperature, and is, thus, unrealistic. In addition, the mutual recombination of point defects at such a vacancy concentration would suppress the damage accumulation, so that the breakaway stage would never take place. Also, single vacancies has to contribute to strains in *c* as well as *a* directions, while the assumption "*that vacancy relaxation is anisotropic and is fully oriented along the c-axis"* with the reference to papers published in nineteen eighties must be erroneous.

The negative *a* strain and coexistence of vacancy- and interstitial-type prismatic loops are the most intriguing parts of the RG phenomenon. Since the *c* strain is always negative, the negative *a* strain violates the basic property of the growth phenomenon: the volume conservation. The coexistence of the loops violates the well-known loop property: vacancy- and interstitial-type loops of large enough size have almost the same efficiencies for absorption of point defects, hence, cannot grow at the same time. This is the reason why their coexistence is never observed in cubic crystals. One may conclude that the negative a strains and coexistence of vacancy and interstitial a loops are fundamental features, specific to hcp crystals.

There were several publications devoted to explaining the coexistence of vacancy and interstitial prismatic loops (see, e.g. [11-13]), all, however, unsuccessful. The main reason was that the models considered Frenkel pairs only, thus ignored the true nature of the primary damage in cascades. In addition, the models [11-13] assumed that both vacancies and SIAs execute 3-D random walk, thus ignored the DAD. Note also that the assumption in [13] that the vacancy dilatation volume is larger than that of SIAs, needed to explain the coexistence, is not supported by *ab initio* calculations (see, e.g. [14]).

The current status of the theory may be summarized by the following citations from the two recent reviews: *"... reliable mechanistic models to predict the deformation of even a pure Zr single crystal are not known … We therefore still rely on a phenomenological approach"* [15], and "*… understanding of the basic creep mechanisms in anisotropic materials like zirconium alloys is still not strong enough to be truly predictive… Today, most models are empirical in nature …"* [16].

The situation described is similar to what it was in the area of void swelling in the bcc- and fcc metals ~20 years ago, the time when the research directions of RG in hcp crystals and void swelling in cubic crystals deviated from each other. Since then, the theory of void swelling has made significant progress in accounting for observations and getting consistent with the experiment and modeling results. The main successes of a new model, the Production Bias Model (PBM), came from including the cascade-production and 1-D migration of the SIA clusters. The PBM explains many striking observations, e.g. the recoil-energy effect, the grain boundary and grain size effects in void swelling, and the void lattice formation, which have been reviewed by Singh *et al.* [17] already more than a decade ago. A recent review one can find in [18].

The displacement cascades and properties of the SIA clusters in hcp Zr are found to be similar to those in cubic materials [19-21]. In addition, the alignment of vacancy loops (see, e.g. [22] and

voids [23,24] along the basal planes observed in irradiated hcp crystals is similar to void ordering in cubic metals, hence the PBM may provide a realistic framework for the damage accumulation in the hcp metals, as well. The aim of the present work is to develop such a model for the RG in Zr.

The paper is organized as follows. In Section 2, the problem is characterized in detail. In Section 3, the model assumptions are listed and the rate equations are formulated. In Section 4, the model predictions are described. Estimates of the maximum strain rate are made in Section 5. Applications of the model for calculations of dose dependence of RG strain are presented in Section 6. A summary is given in Section 7.

2. Problem characterization

In annealed Zr crystals, the RG is characterized by expansion along *a* axes and contraction along *c* axis. A typical strain behavior consists of three distinct stages (see, e.g. [2]). Stage I exhibits a high strain rate and lasts for ~0.1-1.0 dpa (displacements per atom, NRT standard [25]). Stage II demonstrates a very low strain rate, often interpreted as strain saturation, and proceeds up to ~3 dpa. At higher doses, during the stage III, usually referred to as the *breakaway growth* stage, the strain rates increase with increasing dose and reach values as high as $\sim 10^{-3}\text{dpa}^{-1}$. The dose dependence of these rates is debated. The transmission electron microscopy (TEM) exanimation of irradiated samples revealed formation of interstitial-type prismatic loops with the $(1/3)<11\bar{2}0>$ Burgers vectors during stages I and II, and vacancy-type *c* loops during stage III.

In cold-worked materials the strain rates are relatively high from the very beginning and no strain saturation occurs (see, e.g. Fig. 6 in [26]). In some cases, both *a* and *c* strains have been found to be negative. Moreover, the vacancy- and interstitial-type prismatic loops of similar densities and sizes may coexist. To our knowledge, these two observations: the negative *a* strains and coexistence of the vacancy- and interstitial-type prismatic loops have never been explained. Generally, no theory has been published, which explains self-consistently all the observations.

The model presented here gives a self-consistent explanation of the RG phenomenon in Zr single crystals and provides a framework capable of describing all the observations quantitatively.

3. New model

3.1. Basic framework

The model proposed here is a generalization of the PBM developed for cubic crystals to the hcp crystals. The framework for the model, preliminary version of which has been formulated by Golubov *et al.* in [27], is as follows:

- Initial microstructure consists of prismatic and basal edge dislocations.
- The primary radiation damage consists of point defects and SIA clusters.
- Single vacancies and SIAs migrate 3-D.
- The SIA clusters migrate 1-D along $<11\bar{2}0>$ close-packed directions.

- ❖ Interactions of SIA clusters with *c* and *a* dislocations with the Burgers vectors non-parallel to that of the clusters are neglected.
- ❖ The difference in absorption properties of dislocation loops and edge dislocations for mobile point defects and SIA clusters is neglected.
- ❖ The dislocation bias due to interaction of point defects with dislocations/loops and possible anisotropy of single point defects migration is neglected.

The above framework is essentially the PBM [18] adjusted to the hexagonal symmetry of the crystal lattice. The only new assumption is neglecting the interactions of SIA clusters with *c* and *a* dislocations with the Burgers vectors non-parallel to that of the cluster. This originates from the dislocation nature of the interactions, which is qualitatively different from those involving point defects. The interactions depend on mutual orientation of the cluster and dislocation Burgers vectors, which are illustrated in Figs. 1-3 for the interaction energies (see Appendix for calculations). As can be seen from the figures, for basal and prismatic dislocations with non-parallel Burgers vectors, the interactions are significantly weaker than for *a* dislocations with parallel Burgers vectors; while the corresponding trapping zones, associated with the cross-sections of absorption reactions, are significantly smaller. Note that the assumption in question does not affect the results for isotropic distribution of prismatic dislocation Burgers vectors. This is due to symmetry of the cluster production and partitioning in this case: 1/3 part of the SIA clusters are absorbed by *a* dislocations of each particular Burgers vector for any interaction scenario. It does affect the results for non-isotropic distribution of prismatic dislocation Burgers vectors, but the effect must be small for the above-mentioned reason. Accounting for the ignored interactions is straightforward but would lead to a loss of clarity due to a more complicated diffusion-reaction scenario. Note finally that screw dislocations are out of scope of the present model.

3.2. Main equations

The equations for concentrations of mobile defects, single vacancies (subscript v), single SIAs (i) and SIA clusters (cl) in the framework of the model are as follows

$$\frac{dC_{\mathrm{v}}}{dt} = G_{\mathrm{NRT}}(1-\varepsilon_{\mathrm{r}}) - D_{\mathrm{v}}C_{\mathrm{v}}\sum_j \rho_j, \qquad (j = \mathrm{a}_1, \mathrm{a}_2, \mathrm{a}_3, \mathrm{c}) \qquad (1)$$

$$\frac{dC_{\mathrm{i}}}{dt} = G_{\mathrm{NRT}}(1-\varepsilon_{\mathrm{r}})(1-\varepsilon_{\mathrm{i}}^{\mathrm{g}}) - D_{\mathrm{i}}C_{\mathrm{i}}\sum_j \rho_j, \qquad (j = \mathrm{a}_1, \mathrm{a}_2, \mathrm{a}_3, \mathrm{c}) \qquad (2)$$

$$\frac{dC_{\mathrm{cl}}^m}{dt} = G_{\mathrm{NRT}}\frac{(1-\varepsilon_{\mathrm{r}})\varepsilon_{\mathrm{i}}^{\mathrm{g}}}{3n} - D_{\mathrm{cl}}C_{\mathrm{cl}}^m k_m^2, \qquad (m = \mathrm{a}_1, \mathrm{a}_2, \mathrm{a}_3), \qquad (3)$$

where G_{NRT} is the NRT standard value for the defect production rate; ε_{r} is the fraction of defects recombining during the cooling-down phase of a cascade; $\varepsilon_{\mathrm{i}}^{\mathrm{g}}$ and n are the fraction of SIAs survived intra-cascade recombination in the form of clusters and the mean number of SIAs in a cluster, respectively; $D_{\mathrm{v,i}}$ and D_{cl} are the diffusion coefficients of point defects and SIA clusters, respectively; ρ_j are the densities of prismatic dislocations with the Burgers vectors along $\mathbf{a_1}, \mathbf{a_2}, \mathbf{a_3}$, and basal dislocations with the Burgers vector along $\mathbf{c}$ direction; k_m^2 is the sink strength for the SIA clusters migrating along *m* direction. The factor 1/3 on the right-hand side (RHS) of Eq. (3) accounts for the equality of SIA cluster production rates in $\mathbf{a_1}$, $\mathbf{a_2}$ and $\mathbf{a_3}$ directions. The first

terms on the RHSs of Eqs. (1)-(3) stand for the production of defects, while the second terms for their loss at dislocations. The sink strength k_m^2 in Eq. (3) is given by (see, e.g. in [18])

$$k_m^2 = \frac{\pi^2 r_0^2 \rho_m^2}{2}, \qquad (m = \mathrm{a}_1, \mathrm{a}_2, \mathrm{a}_3), \tag{4}$$

where r_0 is the cluster capture radius of prismatic dislocations with the Burgers vectors parallel to that of SIA clusters.

Note that the 3-D migrating point defects are described by the second-order reaction kinetics, so that the sink strengths in Eqs. (1)-(2) are proportional to the total dislocation density, $\rho = \sum_j \rho_j$. In contrast, the 1-D migrating SIA clusters are described by the third-order reaction kinetics, where the sink strength, k_m^2, is proportional to the square of dislocation density. In addition, the sink strength for SIA clusters with a given Burgers vector direction, either $\mathbf{a_1}$, $\mathbf{a_2}$ or $\mathbf{a_3}$, depends on the density of dislocations of the same Burgers vector only. As a result, if the density of $\mathbf{a_1}$ dislocations is, e.g., larger than that of $\mathbf{a_2}$ and $\mathbf{a_3}$, the absorption rate of $\mathbf{a_1}$ dislocations for point defects will be larger. In contrast, the absorption rates of $\mathbf{a_1}$, $\mathbf{a_2}$ and $\mathbf{a_3}$ dislocations for SIA clusters remain the same for any distribution of prismatic dislocations, namely 1/3 of the clusters generated is captured by each type of prismatic dislocations. This is the key difference between 3-D (or preferentially 2-D) diffusing point defects and 1-D diffusing SIA clusters. All the predictions of the model described below follow from this difference.

The steady-state defect fluxes are found by equating the time derivatives in Eqs. (1)-(3) to zero:

$$D_\mathrm{v} C_\mathrm{v} = \frac{G_\mathrm{NRT}\left(1-\varepsilon_\mathrm{r}\right)}{\rho}, \tag{5}$$

$$D_\mathrm{i} C_\mathrm{i} = \frac{G_\mathrm{NRT}\left(1-\varepsilon_\mathrm{r}\right)\left(1-\varepsilon_\mathrm{i}^\mathrm{g}\right)}{\rho}, \tag{6}$$

$$D_\mathrm{cl} C_\mathrm{cl}^m = \frac{2}{3n}\frac{G_\mathrm{NRT}\left(1-\varepsilon_\mathrm{r}\right)\varepsilon_\mathrm{i}^\mathrm{g}}{\pi^2 r_0^2 \rho_m^2}, \quad m = \mathrm{a}_1, \mathrm{a}_2, \mathrm{a}_3, \tag{7}$$

where $\rho = \sum_j \rho_j$ is the total dislocation density. Note that the cluster flux to *c* dislocations is equal to zero.

The dislocation climb velocities, V_j, are defined through the net fluxes of vacancies, single SIAs and SIA clusters to dislocations as

$$V_j = \begin{cases} \dfrac{n}{b_j}\dfrac{D_\mathrm{cl} C_\mathrm{cl}^j k_j^2}{\rho_j} - \dfrac{D_\mathrm{v} C_\mathrm{v} - D_\mathrm{i} C_\mathrm{i}}{b_j}, & j = \mathrm{a}_1, \mathrm{a}_2, \mathrm{a}_3, \\ -\dfrac{1}{b_j}\left(D_\mathrm{v} C_\mathrm{v} - D_\mathrm{i} C_\mathrm{i}\right), & j = \mathrm{c}, \end{cases} \tag{8}$$

where b_j is the Burgers vector of *j*-type dislocations. The strain rate in a particular prismatic direction $\mathbf{a}$, $d\varepsilon_{\mathbf{a}}/d\phi$, due to the climb of prismatic dislocations is calculated by summing contributions from dislocations with different Burgers vectors $(m = \mathbf{a}_1, \mathbf{a}_2, \mathbf{a}_3)$:

$$\begin{aligned}\frac{d\varepsilon_{\mathbf{a}}}{dt} &= \sum_m \rho_m V_m b_m \cos^2\varphi_m = \\ &= \sum_m \left[nD_{\mathrm{cl}} C_{\mathrm{cl}}^m k_m^2 - \rho_m \left(D_{\mathrm{v}} C_{\mathrm{v}} - D_{\mathrm{i}} C_{\mathrm{i}} \right) \right] \cos^2\varphi_m ,\end{aligned} \tag{9}$$

where φ_m is the angle between the vectors $\mathbf{a}$ and $\mathbf{b}_m$. The strain rate in *c* direction is given by

$$\frac{d\varepsilon_{\mathbf{c}}}{dt} = -\rho_c V_c b_c = -\rho_{\mathbf{c}} \left(D_{\mathrm{v}} C_{\mathrm{v}} - D_{\mathrm{i}} C_{\mathrm{i}} \right). \tag{10}$$

By substituting Eqs. (5)-(7) into Eqs. (9) and (10), one finally obtains

$$\frac{d\varepsilon_{\mathbf{a}}}{d\phi} = \chi \sum_m \left(\frac{1}{3} - \frac{\rho_m}{\rho} \right) \cos^2\varphi_m , \tag{11}$$

$$\frac{d\varepsilon_{\mathbf{c}}}{d\phi} = -\chi \frac{\rho_{\mathbf{c}}}{\rho}, \tag{12}$$

where $\phi = G_{\mathrm{NRT}} t$ is the irradiation dose and

$$\chi = (1 - \varepsilon_{\mathrm{r}}) \varepsilon_{\mathrm{i}}^{\mathrm{g}} \tag{13}$$

is the fraction of SIAs at the end of the cooling-down phase of cascades in the clustered form. Note that χ =0 for non-cascade conditions, e.g. for irradiation with ~1 MeV electrons, since the model neglects dislocation bias for point defects.

In a Cartesian coordinate system where *x* axis is along $\mathbf{a}_1$, *y* along $\mathbf{a}_2 - \mathbf{a}_3$, and *z* along $\mathbf{c}$, Eqs. (11) and (12) take the following form

$$\frac{d\varepsilon_{\mathrm{x}}}{d\phi} = \chi \left(\frac{1}{2} - \frac{\rho_{\mathrm{x}}}{\rho} \right), \tag{14}$$

$$\frac{d\varepsilon_{\mathrm{y}}}{d\phi} = \chi \left(\frac{1}{2} - \frac{\rho_{\mathrm{y}}}{\rho} \right), \tag{15}$$

$$\frac{d\varepsilon_{\mathrm{z}}}{d\phi} = -\chi \frac{\rho_{\mathrm{z}}}{\rho}, \tag{16}$$

where

$$\rho_{\mathrm{x}} = \rho_{\mathbf{a}_1} + \left(\rho_{\mathbf{a}_2} + \rho_{\mathbf{a}_3} \right) \cos^2(\pi/3), \tag{17}$$

$$\rho_{\mathrm{y}} = \left(\rho_{\mathbf{a}_2} + \rho_{\mathbf{a}_3} \right) \cos^2(\pi/6), \tag{18}$$

$$\rho_{\mathrm{z}} = \rho_{\mathbf{c}}, \tag{19}$$

$$\rho = \rho_{\mathrm{x}} + \rho_{\mathrm{y}} + \rho_{\mathrm{z}} \equiv \rho_{\mathbf{a}_1} + \rho_{\mathbf{a}_2} + \rho_{\mathbf{a}_3} + \rho_{\mathbf{c}} . \tag{20}$$

Note that Eqs. (14)-(16) can be presented by a diagonal matrix equation as

$$\frac{d\varepsilon_{i,j}}{d\phi} = \chi \left(\frac{1}{2}\left(1 - \delta_{i,3}\right) - \frac{\rho_i}{\rho} \delta_{i,j} \right), \quad (i, j = 1,2,3) , \tag{21}$$

where the indexes 1, 2 and 3 stand for *x*, *y* and *z* , respectively, and $\delta_{i,j}$ is the Kronecker delta. The equations above satisfy the volume conservation

$$\frac{d\varepsilon_x}{d\phi}+\frac{d\varepsilon_y}{d\phi}+\frac{d\varepsilon_z}{d\phi}=0\,, \qquad (22)$$

as it has to be in the absence of swelling.

Eqs. (14)-(16) describe the RG rates as a function of the effective densities of prismatic and basal edge dislocations (including loops), ρ_x, ρ_y, ρ_z, and the parameter χ, which is the fraction of SIAs produced in cascades in the form of 1-D migrating SIA clusters.

4. Model predictions

As can be seen from Eqs. (14)-(16), the strain rates are determined by the fractions of *a* and *c* dislocation densities, ρ_x/ρ, ρ_y/ρ and ρ_z/ρ, rather than by their absolute values. This explains similar strain rates observed in annealed at low irradiation doses and cold-worked materials. In accordance with Eq. (16) the strain rate in *c* direction is always negative. In contrast, the strain rates in *a* directions may be both positive or negative, depending on the distribution of the prismatic dislocation Burgers vectors. The strain rates in prismatic directions are positive for isotropic distribution of prismatic dislocations, i.e. when $\rho_x=\rho_y$. In contrast, the strain rate in *x* direction is negative when $\rho_x/\rho>1/2$ (see Eqs. (14)), i.e. when the distribution of *a* dislocation Burgers vectors is non-isotropic: the inequality is only valid for $\rho_x/\rho_y>1$ at non-zero *c* dislocation density. The *a* strain rates as a function of ρ_x/ρ_y are shown in Fig. 4 for the case $\rho_z/\rho_x=1/5$. As can be seen, the prismatic strain rates, $d\varepsilon_x/d\phi$, $d\varepsilon_y/d\phi$, are positive and equal to each other for isotropic distribution, when $\rho_x/\rho_y=1$, whereas the *x* strain rate is equal to zero at $\rho_x/\rho_y=1.25$ and is negative, of the same order as for *c* direction, at $\rho_x/\rho_y\approx 2$. Thus, the *a* strain rates are sensitive even to small deviations from isotropic distribution of *a* dislocation Burgers vectors. The analysis suggests that the conventional description of the RG in Zr as an expansion along *a* directions and contraction along *c* direction should be changed to an expansion along at least one of *a* directions and contraction along *c* direction. Note also that it follows from Fig. 4 that the absolute values of *a* strain rates increase strongly with increasing ρ_x/ρ_y ratio, while the *c* strain depends only weakly on it. More details on the role of non-uniform distribution of prismatic dislocations on RG are given in Section 4.5.

The upper-bounds of the strain rates are fully determined by the parameter χ, the fraction of SIAs produced in cascades in the clustered form, as described further below in the Section 5.

4.1. Stage I: Initial growth in pre-annealed materials

If the initial densities of *a* dislocations are low, of the order of 10^{12} m^{-2} or less, and the distribution of their Burges vectors is isotropic: $\rho_x^0\approx\rho_y^0$, then $\rho\approx 2\rho_x^0+\rho_z^0\approx 2\rho_x^0$, since the density of *c*

dislocation is normally 5-10 times smaller than that of prismatic dislocations. In this case, it follows from Eqs. (14)-(16) that the initial strain rates are

$$\frac{d\varepsilon_x}{d\phi} \approx \frac{d\varepsilon_y}{d\phi} = \chi\left(\frac{1}{2} - \frac{\rho_x^0}{2\rho_x^0 + \rho_z^0}\right) = \frac{\chi}{4}\frac{\rho_z^0}{\rho_x^0}, \quad (23)$$

$$\frac{d\varepsilon_z}{d\phi} = -\frac{\chi}{2}\frac{\rho_z}{\rho_x^0}. \quad (24)$$

For $\rho_z^0 / \rho_x^0 \approx 0.2$, the strain rate in prismatic direction is equal to $\chi / 20$. To make numerical estimates of the parameter χ for Zr, one needs values for ε_r and ε_i, which are not available due to the lack of systematic studies of cascades in Zr. Since the cascade damage is not drastically sensitive to the type of the lattice, in the following we use the data for neutron-irradiated fcc copper: ε_r=0.9 and ε_i^g =0.2 [28], for which χ=2×10^{-2}. With this value, the strain rates in *a* directions are equal to 10^{-3} dpa^{-1}, which is in a good agreement with observations. Indeed, at this strain rate, the saturation strain, which is found to be of the order 10^{-4} (see, e.g. Fig 3b in [29]), is reached at a dose of ~0.1 dpa, which is close to experiments.

4.2. Stage II: Strain saturation in pre-annealed materials

To understand the reasons for the strain saturation, one needs to take into account that the total density of *a* dislocations is increased with increasing irradiation dose, due to nucleation and growth of *a*-dislocation loops:

$$\rho_{x,y} = \rho_{x,y}^0 + 2\pi R_{x,y} N_{x,y}, \quad (25)$$

where $R_{x,y}$ and $N_{x,y}$ are the radius and number density of corresponding loops. Assuming the distribution of *a*-dislocation loops to be isotropic: $R_x \approx R_y$, $N_x = N_y$, one can find from Eqs. (23) and (24) that the strain rates decrease strongly with the development of loop population. When $2\pi R_{x,y} N_{x,y} >> \rho_{x,y}^0$,

$$\frac{d\varepsilon_x}{d\phi} = \frac{d\varepsilon_y}{d\phi} \approx \frac{\chi}{8\pi}\frac{\rho_z^0}{R_x N_x}, \quad (26)$$

$$\frac{d\varepsilon_z}{d\phi} \approx -\frac{\chi}{4\pi}\frac{\rho_z^0}{R_x N_x}. \quad (27)$$

For values typically observed at the saturation stage: $R_{x,y}$ = 5 nm and $N_{x,y} = 10^{22}\,\mathrm{m}^{-3}$, the sink strength of dislocation loops is equal to 3×10^{14} m^{-2}. Thus, for $\rho_z^0 = 10^{12}$ m^{-2}, the strain rates given by Eqs. (26) and (27) drop down by about 300 times, as compared to those in the beginning of irradiation. With such low strain rates, this stage can be considered as strain saturation, which continues up to ~3 dpa, until the *c* loops start nucleating. In other words, the saturation stage corresponds to a very small but nonzero strain rate.

4.3. Stage III: Breakaway growth

The nucleation and growth of *c* loops leads to an increase of the total sink strength of *c* dislocations:

$$\rho_z = \rho_z^0 + 2\pi R_z N_z \ , \tag{28}$$

hence to an increase of the ρ_z / ρ_x ratio, hence the strain rates. In the case when $2\pi R_z N_z >> \rho_z^0$, the strain rates start to increase as

$$\frac{d\varepsilon_x}{d\phi} \approx \frac{d\varepsilon_y}{d\phi} = \frac{\chi}{8\pi} \frac{\rho_z^0 + 2\pi R_z N_z}{R_x N_x} \approx \frac{\chi}{4} \frac{R_z N_z}{R_x N_x} \ , \tag{29}$$

$$\frac{d\varepsilon_z}{d\phi} = -\frac{\chi}{4\pi} \frac{\rho_z^0 + 2\pi R_z N_z}{R_x N_x} \approx -\frac{\chi}{2} \frac{R_z N_z}{R_x N_x} . \tag{30}$$

Thus, the breakaway strain rates are determined by the ratio $R_z N_z / R_x N_x$, which increases with increasing density and size of *c* loops, in agreement with observations (see, e.g. Figs. 4 in [29]).

4.4. The effect of cold work

The initial dislocation density in cold-worked materials is high, so that the nucleation and growth of *a* loops may not affect the strain rates as strongly as in annealed materials. In the case when $\rho_{x,y}^0$ are significantly smaller than ~10^{14} m^{-2}, the saturation stage may still be identified but less pronounced, because an increase of the total sink strength of *a* dislocations due to nucleation and growth of *a* loops is moderate. At higher dislocation densities, $\rho_{x,y}^0 > 10^{14} m^{-2}$, an increase of the total sink strength of *a* dislocations due to *a* loops becomes so small that saturation of strain does not take place: the initial high strain rate will be maintained, in agreement with observations [29].

4.5. Negative a strains and coexistence of vacancy- and interstitial-type a loops

The models proposed so far all based on the Frenkel-pair production, hence, second-order reaction kinetics, and assume isotropic distributions of *a*-dislocation Burgers vectors. In such models, the driving force for radiation growth is the difference in the efficiencies of vacancy and SIA absorption by *a* and *c* dislocations. The net defect fluxes to *a* and *c* dislocations depend on their total densities and independent on the distribution of *a*-dislocation (and *a*-loop) Burgers vectors. So, if a Frenkel-pair-based model was generalized to account for anisotropy of the distribution, it would give different but nevertheless positive values of *a* strains in different prismatic directions. If an *a* strain were negative in such a model, it would be negative for all *a* directions; then negative *c* strain would violate the volume conservation. In our view, the basic assumption in these models, that the Frenkel pairs are only produced by irradiation, prevented understanding the origin of the negative *a* strain phenomenon. For the same reason, the coexistence of vacancy- and interstitial-type prismatic loops cannot be explained by such models.

The model proposed here predicts negative *a* strain for non-isotropic distribution of *a*-type edge dislocations. To explain the mechanism, let us consider a limiting case, when the density of *a* dislocations with the Burgers vectors along one of the prismatic directions, say *x*, is much larger than the others: $\rho_x >> \rho_y$, and the density of *c* dislocations is much smaller than *a* dislocations, $\rho_z << \rho_x, \rho_y$. In this case, the partitioning of vacancy- and interstitial-type defects is as follows.

The SIA clusters are absorbed equally by both *x* and *y* dislocations; whereas the majority of point defects by *x* dislocations since $\rho_x >> \rho_y$. Because of significant clustering of SIAs, the production rate of single vacancies is higher than single SIAs. As a result, the point defects produce an excess vacancy flux to all dislocations, with the vacancy flux to *x* dislocations larger than to *y* dislocations. Due to equality of SIA cluster absorption by *x* and *y* dislocations, the net vacancy flux is positive to *x* and negative to *y* dislocations, resulting in positive and negative strains in *y* and *x* directions, respectively.

The coexistence of vacancy- and interstitial-type *a* loops occurs for the same reason as the negative *a* strain. This is because the loop absorption properties are similar to those of dislocations, and, as can be seen from Eqs. (25) and (28), the loop nucleation and growth just increase the effective dislocation density. The net vacancy or SIA flux to dislocations, including loops, is equivalent to existence of a super-saturation of corresponding defects that causes nucleation and growth of the corresponding type loops. In the example considered above, the net vacancy flux to *x* dislocations causes nucleation and growth of *x* vacancy loops, while the net SIA flux to *y* dislocations causes nucleation and growth of *y* interstitial loops. Thus, the vacancy-type *x* and interstitial-type *y* loops coexist because they have non-parallel Burgers vectors. Their contributions to strains are not additive for the same reason. This explains why the contraction in *c* direction takes place even when the size and density of vacancy loops are similar to or even larger than those of interstitial loops: the negative strains in one of *a* directions and *c* direction are compensated by corresponding positive strain in another *a* direction.

Note that, due to hexagonal symmetry, different orientations of the vacancy and interstitial loops should not be obvious from an ordinary examination of the microstructure, since TEM observation of arbitrarily-orientated sample would show both vacancy- and interstitial-type loops at the same time. These may be revealed for special orientations of the sample; if, e.g., vacancy loop Burgers vectors are all parallel to a_1 direction, they will be invisible for orientations perpendicular to a_1.

It should be emphasized that the explanation of the negative *a* strain proposed is based on non-isotropic distribution of edge *a* dislocations, the significance of which has never been emphasized before, and which has never been subjected to measurements. For example, in the paper by Zee *et al.* [26], where the negative *a* strain was observed in a single Zr crystal pre-strained along an axis close to one of *a* directions, the total density of dislocations was reported only. Moreover, the fractions of edge and screw dislocations are unknown. So, a comparison of the model with the experiment is not possible.

The dislocation structure in deformed Zr crystals has proved to be complicated (see, e.g. [30]), and the information needed may hardly be predicted. For example, estimations of the Schmidt factors for experimental conditions in [26] show that most favorable slip planes for prismatic dislocations will be in the directions non-parallel to the loading direction. This does not favor the production of dislocations with the Burgers vector parallel to the loading direction required in the present model. However, such an analysis does not take into account evolution of screw dislocation structure during tensile straining and their effect on the distribution of edge dislocations. In addition, the dislocation density after deformation measured in [26] is as low as

$2x10^{12}$ m^{-2}, which is of the same order as in a non-deformed crystal. This makes it difficult to speculate on the real structure of edge *a* dislocations after deformation.

4.6. Alignment of vacancy-type defects

A planar alignment of the vacancy-type loops and voids in *c* planes observed in neutron-irradiated hcp metals [22] is analogous to void ordering in cubic metals and must have the same origin, which is due to interaction of voids and loops with the SIA clusters diffusing 1-D along close-packed crystallographic directions (see refs. in [17]). At a high temperature corresponding to the void-swelling regime, the void alignment in hcp metals must be driven by the SIA cluster-void interactions. At low temperature, the alignment of *c*-type vacancy loops must also be due to interaction with the SIA clusters, but the exact ordering mechanism is not yet clear. There are, at least, two possibilities: (a) via complete annihilation of unaligned loops, or (b) by the loop repulsion by moving SIA clusters. Modeling by MD may clarify the issue.

Note that the planar alignment of the vacancy-type defects was also found in Zr under 1 MeV electron irradiation [24], i.e. in an absence of displacement cascades. It seems reasonable to associate it with the preferential migration of single SIAs in the basal plane, as in the DAD model. However, anisotropic vacancy diffusion revealed in *ab initio* calculations [14] jeopardizes this explanation. The 1-D diffusion of small, containing few SIAs, clusters formed kinetically may be another possibility. Detailed analysis of this case, however, is out of scope of the present study. Multi-scale simulations are required to clarify the issue.

5. Estimates of strain rates

5.1. Absolute maximum

It follows from Eqs. (14)-(16) that one of the limiting cases for the strain rates may be achieved when the density of *c* dislocations is very high: $\rho_z / \rho \to 1$ and $\rho_{x,y} / \rho \to 0$. In this case

$$\left(\frac{d\varepsilon_x}{d\phi}\right)_{max} \approx \left(\frac{d\varepsilon_y}{d\phi}\right)_{max} \approx \frac{\chi}{2}, \tag{31}$$

$$\left(\frac{d\varepsilon_z}{d\phi}\right)_{max} \approx -\chi\,. \tag{32}$$

High rates may also be realized in the opposite case, when the density of *c* dislocations is relatively small: $\rho_z << \rho_x, \rho_y$, but ρ_x and ρ_y are very different, e.g. $\rho_x >> \rho_y$. In this case

$$\left(\frac{d\varepsilon_x}{d\phi}\right)_{max} \approx -\left(\frac{d\varepsilon_y}{d\phi}\right)_{max} \approx \frac{\chi}{2}\,, \tag{33}$$

$$\left(\frac{d\varepsilon_z}{d\phi}\right) \approx 0\,. \tag{34}$$

As can be seen from Eqs. (31)-(34), in both cases the *a*-strain rates are fully determined by the properties of cascades. Taking the value of χ equal to 2×10^{-2} (see Section 4.1 for explanation), one may estimate the *a*-strain rate to be of the order of 10^{-2} dpa^{-1} (1%/dpa), which is the same as the

maximum swelling rate in fcc metals and austenitic stainless steels. Such a coincidence could not be accidental, but must reflect similarity of the cascades in metallic material, particularly with fcc and hcp structures, and mechanisms operating under cascade damage conditions.

Note, however, that the first case considered above is not realistic in Zr-based materials, because the density of *c* dislocations is normally significantly smaller than that of *a* dislocations. The second case is more realistic but, to our knowledge, such a high strain rate has not been reported yet.

5.2. Isotropic distribution of dislocations

For isotropic distribution of dislocation Burgers vectors: $\rho_{\mathrm{x}} = \rho_{\mathrm{y}} = \rho_{\mathrm{z}}$, Eqs. (14)-(16) give

$$\left(\frac{d\varepsilon_{\mathrm{x}}}{d\phi}\right) = \left(\frac{d\varepsilon_{\mathrm{y}}}{d\phi}\right) = \frac{\chi}{6}, \tag{35}$$

$$\left(\frac{d\varepsilon_{\mathrm{z}}}{d\phi}\right) = -\frac{\chi}{3}. \tag{36}$$

The strain rates are three times smaller than the maximum values given by Eqs. (31) and (32), but still about three times higher than ~10^{-3} dpa^{-1} observed. The realistic strain rates are predicted by the model when the difference between densities of *c* and *a* dislocations is taken into consideration: $\rho_{\mathrm{z}} < \rho_{\mathrm{x}}, \rho_{\mathrm{y}}$, which, according to Eq. (16) , reduces the *c* and *a* strains. For example, in the case when $\rho_{\mathrm{z}} = \left(\rho_{\mathrm{x}} + \rho_{y}\right)/5$ and $\rho_{\mathrm{y}} = \rho_{\mathrm{x}}$, which is usual in Zr materials, the *a*-strain rates are ~10^{-3} dpa^{-1} which fit well the observations.

6. Dose dependence of growth strains

The analysis presented in the previous two sections is based on Eqs. (14) and (16) for the instantaneous strain rates in a crystal with given dislocation structure. With increasing dose, the total dislocation densities change due to nucleation and growth of dislocation loops:

$$\rho_{\mathrm{x,y,z}}(\phi) = \rho^{0}_{\mathrm{x,y,z}} + 2\pi R_{\mathrm{x,y,z}}(\phi) N_{\mathrm{x,y,z}}(\phi), \tag{37}$$

where ρ^{0} are the initial dislocation densities, and R and N are the radii and densities of *a* and *c* loops. To calculate the dose dependence of strains, one needs to know the dose dependences of the loop radii and densities.

The loop radii are described by equations similar to Eqs. (8) for dislocation climb velocities. For loops with particular Burgers vectors:

$$\begin{aligned} \frac{dR^{\mathrm{a}}_{j}}{dt} &= \frac{n}{b_j}\frac{D_{\mathrm{cl}}C^{j}_{\mathrm{cl}}k^{2}_{j}}{\rho_j} - \frac{D_{\mathrm{v}}C_{\mathrm{v}} - D_{\mathrm{i}}C_{\mathrm{i}}}{b_j}, \qquad j = \mathrm{a}_1, \mathrm{a}_2, \mathrm{a}_3, \\ \frac{dR^{\mathrm{c}}}{dt} &= \frac{1}{b_{\mathrm{c}}}\left(D_{\mathrm{v}}C_{\mathrm{v}} - D_{\mathrm{i}}C_{\mathrm{i}}\right). \end{aligned} \tag{38}$$

The equations for the effective radiuses of *a* loops in the Cartesian coordinate system, $R_{\mathrm{x,y}}(\phi)$, can be obtained from Eq. (38) by using equations similar to Eqs. (17) and (18), which connect the effective dislocation densities with those in particular crystallographic directions.

The situation with the nucleation of loops is more difficult because not much is known. Available experimental data can be summarized as follows: (a) *a* loops nucleate from the very beginning of irradiation and reach the density of ~10^{22} m^{-3} after several dpa, (b) *c* loops start nucleating at a dose of ~3 dpa and reach an order of magnitude smaller density, ~10^{21} m^{-3} . The nucleation mechanisms of *a* and *c* loops are out of scope of the present work. In this paper, we use the loop nucleation scenario shown in Fig. 5, which has been derived from observations (see the next section). By using Eqs. (38), the dose dependence of the growth strain has been calculated by a computer code RIMD-ZR.V1 (Radiation-Induced Microstructure and Deformation of Zr, Version 1) developed by the authors (see details in [31]). Selected calculations are presented below.

6.1. Radiation growth in annealed materials

As a first step, we fit the nucleation scenario (Fig. 6) to the experimental data from [29] for low-dose neutron irradiation of annealed Zr crystals, using $\chi = 2\times10^{-2}$ and 10^{12} m^{-2} for the initial densities of *a* dislocations of all three prismatic directions, and two times smaller value for *c* dislocation. The best-fit results together with the experimental data are presented in Fig. 6, and demonstrate excellent agreement. Then, the calculations have been continued to larger doses, for which the results are shown on Fig. 7. As can be seen, the calculations reproduce all the three stages observed: fast initial growth, strain saturation and the breakaway growth.

6.2. Effect of cold work

The effect of cold work has been investigated by changing the initial dislocation density by three orders of magnitude: from 3×10^{12} to 3×10^{15} m^{-2}, with the description of the loop nucleation shown on Fig. 5. The results are presented in Fig. 8. As can be seen, an increase of dislocation density leads to a qualitative change in the strain behavior: now, a high strain rate ~10^{-3} dpa^{-1} is maintained from the very beginning of irradiation. This is in a good agreement with experiments (see, e.g. [29]).

6.3. RG at high doses

The results shown in Figs. 7 and 8 have been obtained for relatively low doses, < 10 dpa, which allows comparing with observations available. A more practically important issue is the dose dependence on the breakaway stage, at doses beyond existing databases. An analytical study [31] predicts constant strain rates at high irradiation doses, determined by the number densities of *a* and *c* loops. The calculations for up to 100 dpa are presented in Fig. 9. As can be seen, the results reproduce analytical predictions, and demonstrate the sensitivity to the ratio of the *a*- and *c*-loop densities: the higher the ratio the smaller the strain rate, which is proportional to $\left(N_{ic} / N_{ia}\right)^{1/2}$. It follows from the model that the growth strain at high doses can be predicted from the microstructure at end of the loop nucleation period.

6.4. Coexistence of vacancy and interstitial a loops

The calculation results presented above have been obtained for isotropic distribution of *a*-dislocation Burgers vectors. In this case, the RG exhibit usual behavior, i.e. expansion in *a* directions and contraction in *c* direction. The results presented in Fig. 10 have been obtained for the case when the distribution of *a* dislocations is not isotropic, namely the density of dislocations with the Burgers vectors parallel to $\mathbf{a}_1$ is five times higher than those with the Burgers vectors along $\mathbf{a}_2$ and $\mathbf{a}_3$. The nucleation of *a* loops is described using a commonly accepted scheme, where the vacancy loops are nucleated for positive and interstitial loops for negative net vacancy flux to the loop embryos. As can be seen from the figure, the strain rate in *x* direction (parallel to $\mathbf{a}_1$) is negative, i.e. in the direction of the highest dislocation density, in accordance with the discussion in Section 4.5. The negative *a* strain takes place until ~4 dpa, making distribution of *a*-dislocation Burgers vectors more isotropic, and the strain becomes positive. The change of the negative *a* strain to positive with increasing dose has been observed [2], so that our calculations agree with experimental observations. Finally, we note that negative *a* strains have to be quite common within certain dose range, because the probability of isotropic distribution of *a*-dislocation Burgers vectors in cold-worked samples is quite small.

7. Summary

A model of radiation growth of Zr single crystals under neutron irradiation has been developed, which takes into account the true nature of the primary damage in cascades of atomic displacements, and the diffusion properties of SIA clusters. The model contains one parameter only, that is, the fraction of SIAs produced in cascades in the form of clusters, which has been estimated from MD results and experiments. The model explains all the major observations in Zr including strain saturation, breakaway growth, the effect of cold work, negative *a* strain and coexistence of vacancy and interstitial prismatic loops.

The main model predictions can be summarized as follows:

- The strains in prismatic directions are positive for isotropic distribution of prismatic dislocation Burgers vectors.
- The maximum strain rate in this case is estimated to be ~10^{-3} dpa^{-1}, in accordance with experiment.
- For the first time, the linear dose dependence of the growth strain in the breakaway stage is predicted at high doses. The corresponding rate can be calculated from the microstructure at intermediate doses.
- It has been shown for the first time that the anisotropy of distribution of prismatic dislocations is an important factor determining strain behavior.
- Observations of negative *a* strain and co-existence of vacancy and interstitial prismatic loops are both explained for the first time. It is shown that both these phenomena originate from anisotropy of prismatic dislocation Burgers vectors.
- The absolute maximum of the strain rate is estimated to be ~10^{-2} dpa^{-1}. In particular, it may be realized at significant anisotropy of prismatic dislocation Burgers vectors and relatively small density of *c* dislocations.

It should be mentioned that the absolute maximum growth strain rate predicted by the model is of the same order as the maximum swelling rate observed in cubic metals and predicted by

the PBM (see refs. in [18]). This indicates that the mechanisms governing damage accumulation in cubic and hcp crystals are similar. Thus, the PBM, developed initially for cubic metals, provides, in fact, general framework for the description of radiation effects in metallic materials.

Acknowledgements

This research was supported by the Consortium for Advanced Simulation of Light Water Reactors (http://www.casl.gov), an Energy Innovation Hub (http://www.energy.gov/hubs) for Modeling and Simulation of Nuclear Reactors under U.S. Department of Energy Contract No. DE-AC05-00OR2272.

References

1. S.N. Buckley, Properties of Reactor Materials and Effects of Radiation Damage, ed. W.J. Littler (Butterworths, London, 1962), p. 413.
2. R.A. Holt, Mechanisms of irradiation growth of alpha-zirconium alloys, J. Nucl. Mater. 159 (1988) 310.
3. C.H. Woo, U.M. Gösele, Dislocation bias in an anisotropic diffusive medium and irradiation growth, J. Nucl. Mater. 119 (1983) 219.
4. C.H. Woo, Theory of irradiation deformation in non-cubic metals: effects of anisotropic diffusion, J. Nucl. Mater. 159 (1988) 237.
5. B. von Guerard, J. Peisl, Agglomeration of point defects in copper after neutron irradiation at 4-6 K, J. Appl. Cryst. 8 (1975) 161.
6. R.E. Stoller, Primary radiation damage formation (2012), In: Konings R.J.M. (ed.) Comprehensive Nuclear Materials V. 1, pp. 293-332, Amsterdam: Elsevier.
7. R.A. Holt, C.H. Woo, C.K. Chow, Production bias - A potential driving force for irradiation growth, J. Nucl. Mater. 205 (1993) 293.
8. F. Christien, A. Barbu, Cluster Dynamics modeling of irradiation growth of zirconium single crystals, J. Nucl. Mater. 393 (2009) 153.
9. W.G. Wolfer, A. Si-Ahmed, The effect of nonlinear elasticity on the capture efficiency of dislocation loops, Phys. Lett. 76A (1980) 341.
10. G. Samolyuk, Y.N. Osetsky, S.I. Golubov, R. Stoller, SIA in hcp Zr. Formation energies, barriers, MRS-fall meeting, Boston, November 2012 (in preparation).
11. M. Christensen, W. Wolf, C. Freeman, E. Wimmer, R.B. Adamson, L. Hallstadius, P. Cantonwine, E. V. Mader, Effect of hydrogen on dimensional changes of zirconium and the influence of alloying elements: first-principles and classical simulations of point defects, dislocation loops, and hydrides, ASTM conference proceedings of 17th International Symposium on Zirconium in the Nuclear Industry, Hyderabad, India (in preparation).
12. C.H. Woo, Intrinsic bias differential between vacancy loops and interstitial loops, J. Nucl. Mater. 107 (1982) 20.
13. V.I. Dubinko, A.S. Abyzov, A.A. Turkin, Numerical evaluation of the dislocation loop bias, J. Nucl. Mater. 336 (2005) 11.
14. G. Vérité, F. Willaime, C.C. Fu, Anisotropy of the vacancy migration in Ti, Zr and Hf hexagonal close-packed metals from first principals, Solid State Phenomena 129 (2007) 75.
15. R.A. Holt, In-reactor deformation of cold-worked Zr–2.5Nb pressure tubes**,** J. Nucl. Mater. 372 (2008) 182.
16. R. Adamson, F. Garzarolli, C. Patterson, In-reactor creep of Zirconium Alloys, *Advance Nuclear Technology International* (2009), Krongjutarvägen 2C, SE-730 50 Skultuna Sweden.
17. B.N. Singh, H. Trinkaus, S.I. Golubov, "Radiation Damage Theory", Encycl. of Mater.: Science and Techn. ISBN: 0-08-0431526 (2001) 7957.
18. S.I. Golubov, A.V. Barashev, R.E. Stoller, Radiation damage theory. In: Konings R.J.M., (ed.) Comprehensive Nuclear Materials, volume 1, pp. 357-391, Amsterdam, 2012: Elsevier.
19. S.J. Wooding, L.M. Howe, F. Gao, A.F. Calder, D.J. Bacon, A molecular dynamics study

of high-energy displacement cascades in α-Zirconium, J. Nucl. Mater. 254 (1998) 191.
20. N. De Diego, Y.N. Osetsky, D.J. Bacon, Mobility of interstitial clusters in HCP Zirconium, In: Proceedings of MRS Fall Meeting; Boston, MA; USA; (2000) p. 200.
21. N. De Diego, Y.N. Osetsky, D.J. Bacon, Structure and properties of vacancy and interstitial clusters in α-Zirconium, J. Nucl. Mater. 374 (2008) 87.
22. M. Griffiths, R.A. Holt, A. Rogerson, Microstructural aspects of accelerated deformation of Zircaloy nuclear reactor components during service, J. Nucl. Mater. 225 (1995) 245.
23. R. Risbet, V. Levy, Ordre de cavites dans le magagnesium et l'aluminium irradies aux neutrons rapides, J. Nucl. Mater. 50 (1974) 116.
24. Y. de Carlan, C. Regnard, M. Griffiths, D. Gilbon, C. Lemaignan, Influence of iron in the nucleation of <c> component dislocation loops in irradiated Zircaloy-4, ASTM STP 1295 (1996) 638.
25. M.J. Norgett, M.T. Robinson, I.M. Torrens, A proposed method of calculating displacement dose rates, Nucl. Eng. Des. 33 (1975) 50.
26. R.H. Zee, G.J.C. Carpenter, A. Rogerson, J.F. Walters, Irradiation growth in deformed zirconium, J. Nucl. Mater. 150 (1987) 319.
27. S.I. Golubov, A.V. Barashev, R.E. Stoller, On the origin of radiation growth of hcp crystals, ORNL/TM-2011/473.
28. S.I. Golubov, B.N. Singh, H. Trinkaus, On recoil-energy-dependent defect accumulation in pure Copper. Part II. Theoretical treatment, Phil. Mag. A81 (2001) 2533.
29. G.J.C. Carpenter, A. Rogerson, R.H. Zee, Irradiation growth of zirconium single crystals: A review, J. Nucl. Mater. 159 (1988) 86.
30. A. Akhtar, A. Teghtsoonian, Plastic deformation of zirconium single crystals, Acta Metallurgica 19 (1971) 655.
31. A.V. Barashev, S.I. Golubov, R.E. Stoller, Theoretical investigation of microstructure evolution and deformation of zirconium under cascade damage conditions, ORNL Report: ORNL/TM -2012/225 (2012).
32. M.J. Makin, The long-range forces between dislocation loops and dislocations, Phil. Mag. 106 (1964) 695.

Appendix

The interaction between a dislocation loop and an edge dislocation depends strongly on their mutual orientation. This was analyzed by Makin [32] using infinitesimal loop approximation in the framework of the isotropic elasticity theory. The corresponding interaction energy can readily be obtained with the aid of Eqs. (1) in [32] for the components of the stress tensor, σ_{ij}, as

$$E = A\sum_{i,j}\sigma_{ij}b_i n_j, \qquad \text{(A1)}$$

where b_i is the component of the cluster Burgers vector on *i* direction and An_j is the area of the loop resolved onto a plane perpendicular to the *j* direction. The result is as follows.

Consider a Cartesian coordinate system with x_1, x_2 and x_3 axes and a straight edge dislocation with its line along x_3 direction (line sense) and the Burgers vector along x_1, and distinguish two cases. The first case represents an *a*-type dislocation with the Burgers vector b_a; the SIA cluster moves in the plane perpendicular to x_3 direction, hence containing x_1 and x_2 vectors and its Burgers vector is at an angle α to the dislocation Burgers vector and x_1. The interaction energy in this case is defined by the following equation:

$$E_a = \frac{E_0 b_a n}{\left(x_1^2 + x_2^2\right)^2}\left[-x_2\left(3x_1^2 + x_2^2\right)\cos^2\alpha + 2x_1\left(x_1^2 - x_2^2\right)\cos\alpha\sin\alpha + x_2\left(x_1^2 - x_2^2\right)\sin^2\alpha\right], \qquad \text{(A2)}$$

where $E_0 = \mu\Omega/2\pi(1-\nu)$; μ is the shear modulus, ν is the Poisson ratio, Ω is the atomic volume, and *n* is the number of SIAs in the loop, which enters via the relationship $Ab = \Omega n$.

When the Burgers vectors of an SIA cluster and an *a* dislocation are parallel to each other, Eq. (A2) is reduced to the following equation:

$$E_a\left(\alpha = 0\right) = -E_0 b_a n \frac{x_2\left(3x_1^2 + x_2^2\right)}{\left(x_1^2 + x_2^2\right)^2}. \qquad \text{(A3)}$$

In this case, the Burgers vectors of an SIA cluster and an *a* dislocation are non-parallel, $\alpha=\pi/3$, Eq. (A2) is reduced to

$$E_a\left(\alpha = \frac{\pi}{3}\right) = \frac{E_0 b_a n}{\left(x_1^2 + x_2^2\right)^2}\left[-\frac{x_2}{4}\left(3x_1^2 + x_2^2\right) + \frac{\sqrt{3}}{2}\left(x_1 + \frac{\sqrt{3}}{2}x_2\right)\left(x_1^2 - x_2^2\right)\right]. \qquad \text{(A4)}$$

The second case corresponds to the *c*-type dislocation with the Burgers vector b_c. In this case, the SIA cluster moves in the plane perpendicular to x_1 direction, hence containing x_3 and x_2 vectors, and its Burgers vector is at an angle β to the dislocation line and x_3. The interaction energy in this case is given by

$$E_c = \frac{E_0 b_c n}{\left(x_1^2 + x_2^2\right)^2}\left[x_2\left(x_1^2 - x_2^2\right)\sin^2\beta - 2\nu x_2\left(x_1^2 + x_2^2\right)\cos^2\beta\right]. \qquad \text{(A5)}$$

In the case when cluster Burgers vector is perpendicular to that of the dislocation line, $\beta = \pi/2$, Eq. (A5) is reduced to the following equation:

$$E_c\left(\beta=\frac{\pi}{2}\right)=E_0 b_c n\frac{x_2\left(x_1^2-x_2^2\right)}{(x_1^2+x_2^2)^2}. \qquad \text{(A6)}$$

Eqs. (A3), (A4) and (A6) allow calculating the cluster-dislocation interaction energy, E, and corresponding trapping zones: areas with the binding energy ($-E$) higher than the thermal energy, $k_B T$, where k_B is the Boltzmann constant and T the absolute temperature. Figs. 1 to 3 show the interaction energy between an edge dislocation and a 10-SIA cluster in Zr at 573K for three cases: (1) an *a* dislocation with the Burgers vector parallel to that of the cluster, (2) an *a* dislocation with the Burgers vector at $2\pi/3$ angle to that of the cluster, and (3) a *c* dislocation with the Burgers vector perpendicular to that of the cluster. Each figure shows three regions: the capture zone (grey) where $E \le -k_B\mathrm{T}$, the repulsion zone (dark) where $E > k_B\mathrm{T}$, and an intermediate region where $E \approx 0$ (bright gray). The calculations were performed with μ = 66 GPa, ν=0.34, Ω= 2.33x10^{-29} m^{-3}, for which E_0 = 2.01 eV. As can be seen from the figures, the cross-section of the capture zone (perpendicular to the cluster motion direction along its Burgers vector) in the first case (parallel Burgers vectors of the cluster and dislocation) is the largest, ~250*b*. The other two cases are characterized by significantly smaller the interaction cross-sections and weaker interaction. This is the reason for the simplifying assumption in the model, which ignores relatively weak interactions of the clusters and *a* dislocations with non-parallel Burgers vectors and *c* dislocations.

Figure captions

Figure 1. Interaction energy between an *a* dislocation with the Burgers vector parallel to that of a 10-SIA cluster in Zr at 573K. The dislocation line is at the coordinate origin and perpendicular to the (x_1,x_2) plane. x_1 is the distance from dislocation extra plane, along the dislocation Burgers vector (shown in the figure). x_2 is the distance from the dislocation line, along the direction perpendicular to the dislocation Burgers vector. The cluster Burgers vector is shown in the figure as $\boldsymbol{b}_{\mathrm{cl}}$.

Figure 2. Same as in Fig. 1 but for *a* dislocation with the Burgers vector at $2\pi/3$ angle to that of the cluster.

Figure 3. Same as in Fig. 1 but for *c* dislocation with the Burgers vector perpendicular to that of the cluster.

Figure 4. Effect of non-uniform distribution of *a* dislocation Burgers vectors on strain rates in the case when density of *c* dislocations is five times smaller than *a* dislocations. Note that *x* strain becomes negative at $\rho_x / \rho_y > 1.25$ and reaches the strain rate of *c* dislocations at $\rho_x / \rho_y = 2.5$.

Figure 5. Vacancy and interstitial loop nucleation scenario.

Figure 6. Best-fit calculations and experimental measurements from [29].

Figure 7. Growth strain in a wider dose range.

Figure 8. Effect of cold work on growth strain behavior.

Figure 9. Growth strain behavior at very high doses.

Figure 10. Growth strain behavior for anisotropic distribution of *a*-dislocation Burgers vectors.

Figure 1

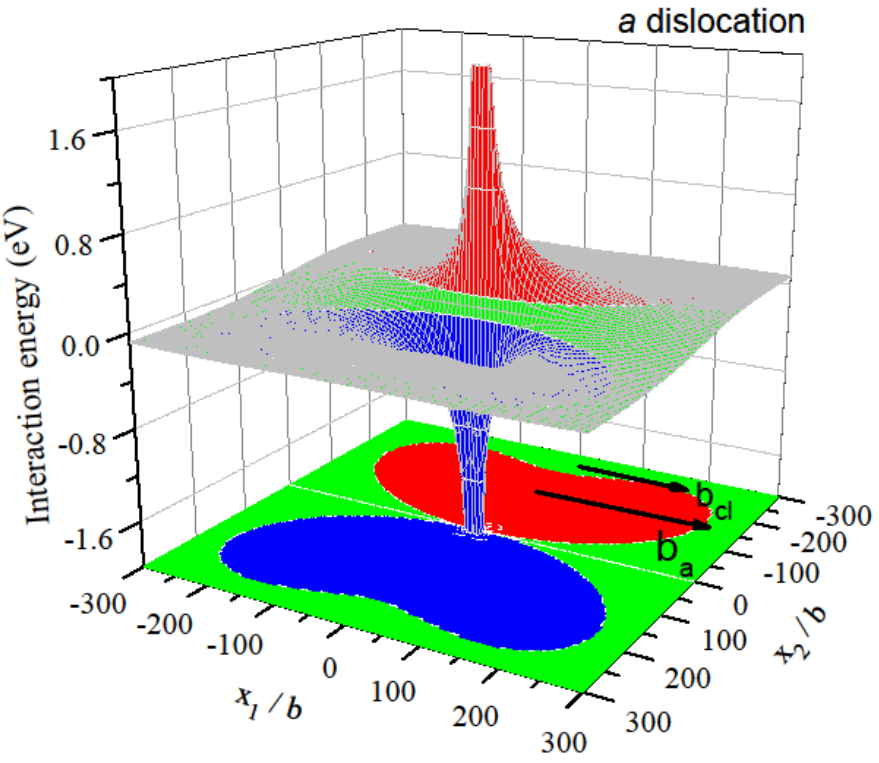
a dislocation
Interaction energy (eV)
1.6
0.8
0.0
-0.8
-1.6
-300
-200
-100
0
100
200
300
x_1 / b
x_2 / b
b_{cl}
b_a

Figure 2

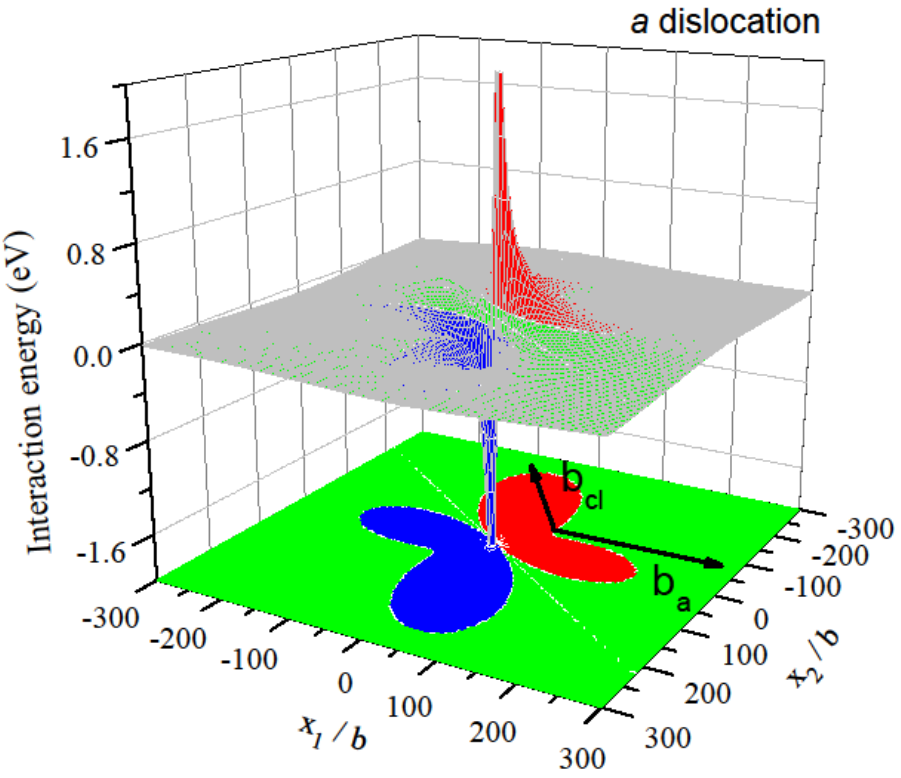
a dislocation
Interaction energy (eV)
1.6
0.8
0.0
-0.8
-1.6
-300
-200
-100
0
100
200
300
x_1 / b
x_2 / b
b_{cl}
b_a

Figure 3

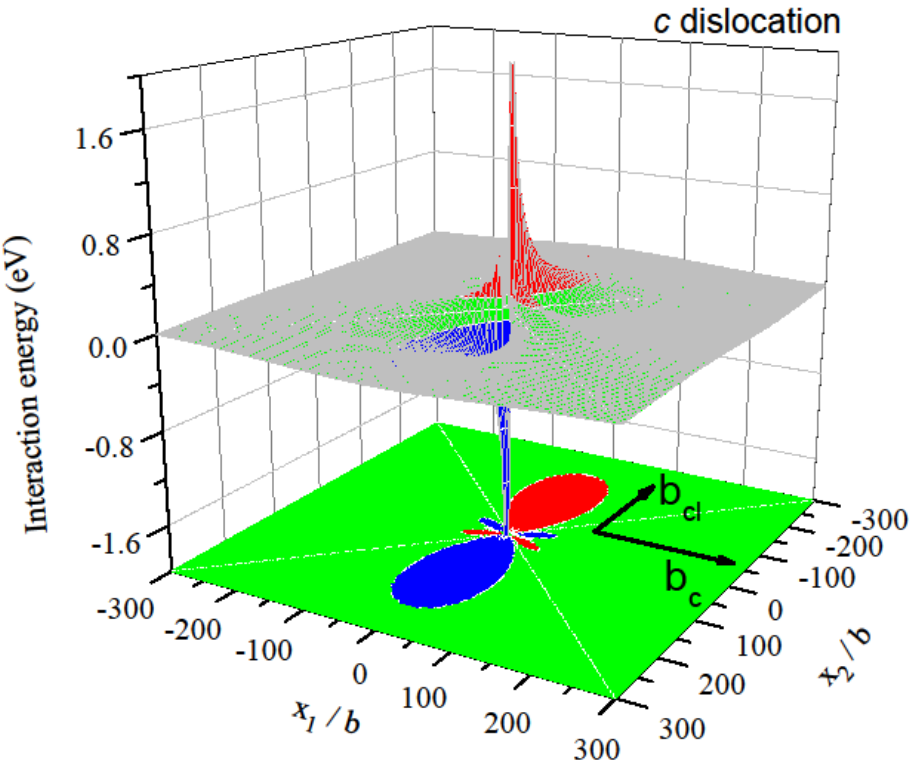
c dislocation
Interaction energy (eV)
1.6
0.8
0.0
-0.8
-1.6
-300
-200
-100
0
100
200
300
x_1 / b
x_2 / b
b_{cl}
b_c

Figure 4

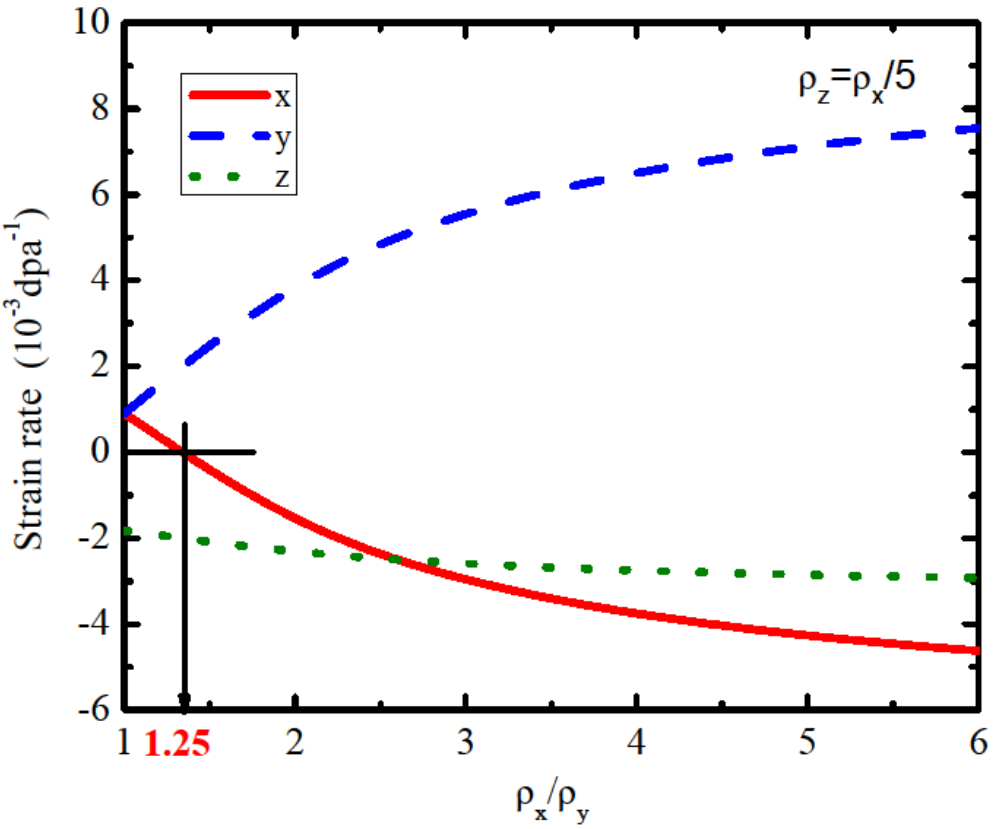
10
8
6
4
2
0
-2
-4
-6
1
1.25
2
3
4
5
6
x
y
z
$\rho_z=\rho_x/5$
Strain rate (10^{-3}dpa^{-1})
ρ_x/ρ_y

Figure 5

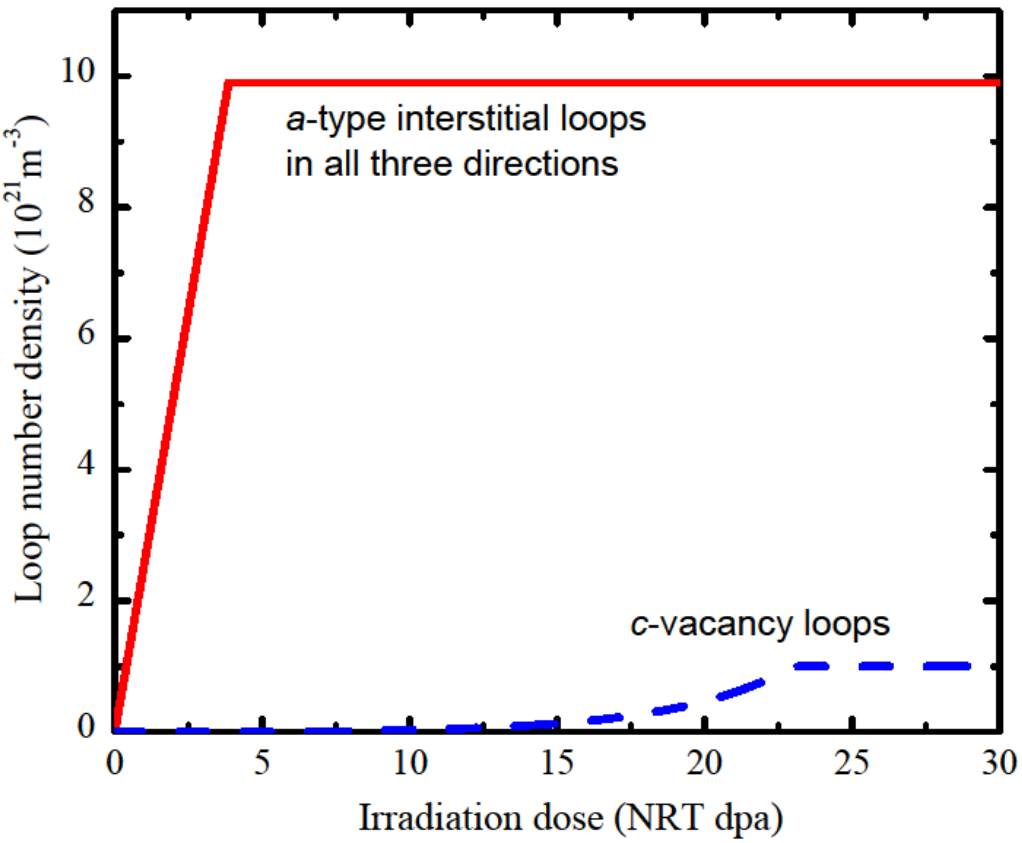
a-type interstitial loops
in all three directions
c-vacancy loops
Loop number density (10^{21}m^{-3})
Irradiation dose (NRT dpa)
0
2
4
6
8
10
0
5
10
15
20
25
30

Figure 6

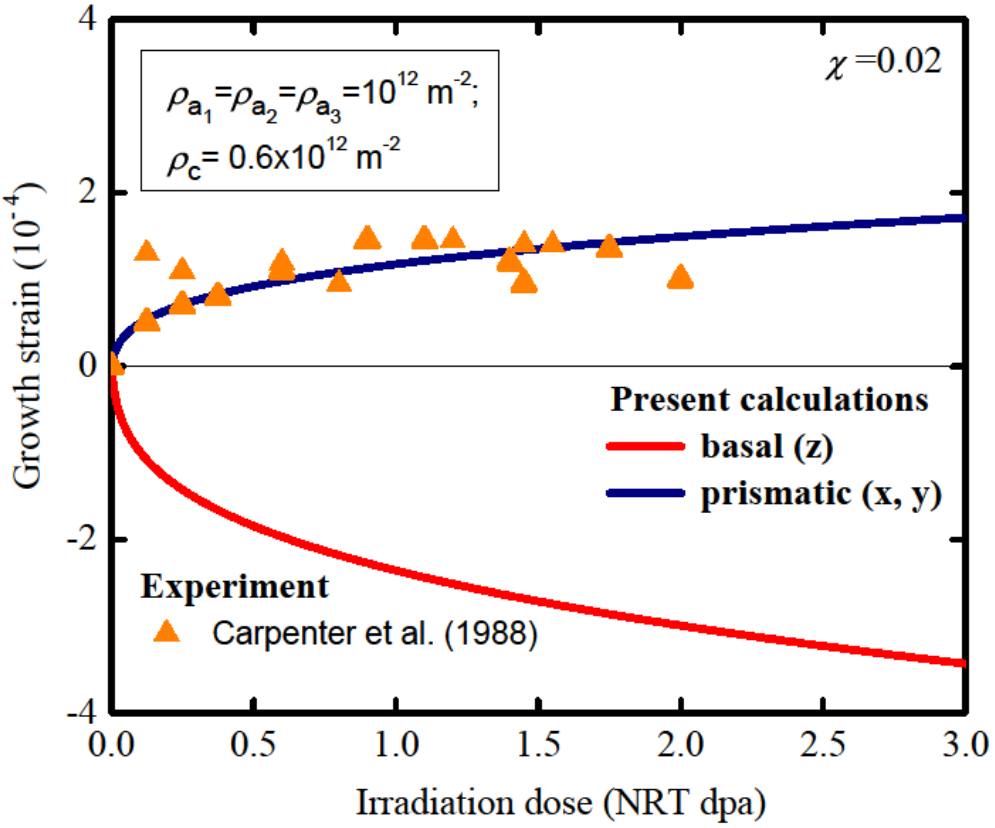
$\rho_{a_1}=\rho_{a_2}=\rho_{a_3}=10^{12}$ m^{-2};
$\rho_c= 0.6\text{x}10^{12}$ m^{-2}
χ =0.02
Present calculations
basal (z)
prismatic (x, y)
Experiment
Carpenter et al. (1988)
Growth strain (10^{-4})
Irradiation dose (NRT dpa)
4
2
0
-2
-4
0.0
0.5
1.0
1.5
2.0
2.5
3.0

Figure 7

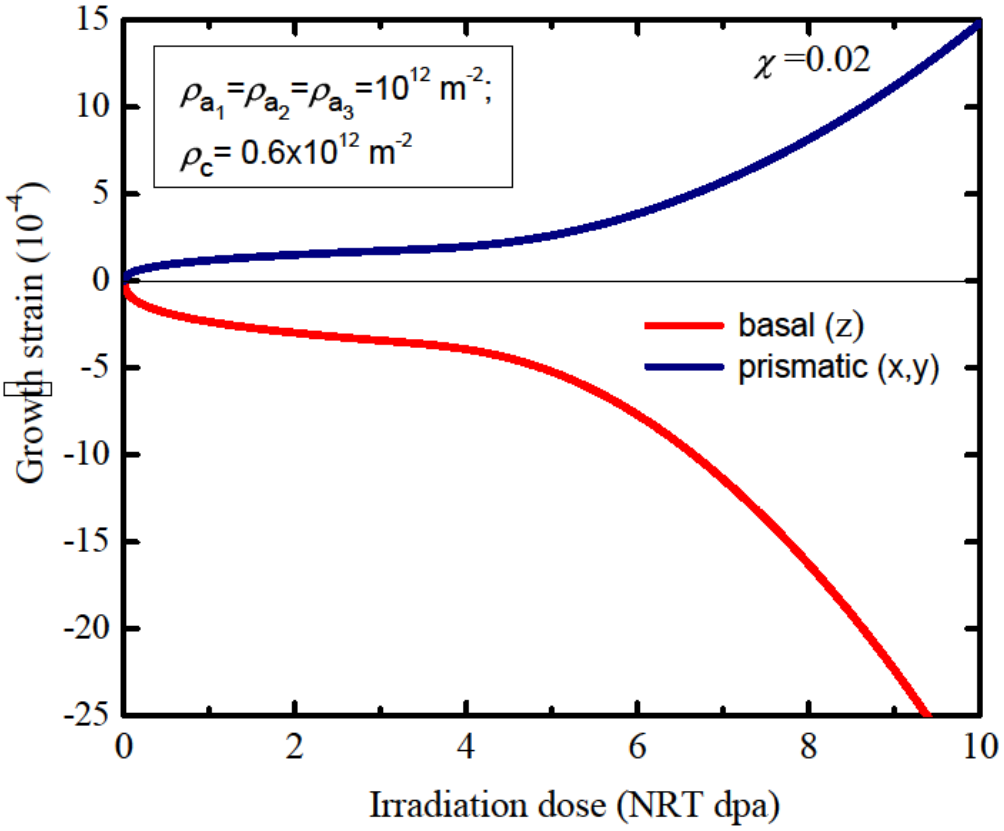
15
10
5
0
-5
-10
-15
-20
-25
0
2
4
6
8
10
Growth strain (10^{-4})
Irradiation dose (NRT dpa)
$\rho_{a_1}=\rho_{a_2}=\rho_{a_3}=10^{12}$ m^{-2};
$\rho_c= 0.6\text{x}10^{12}$ m^{-2}
χ =0.02
basal (z)
prismatic (x,y)

Figure 8

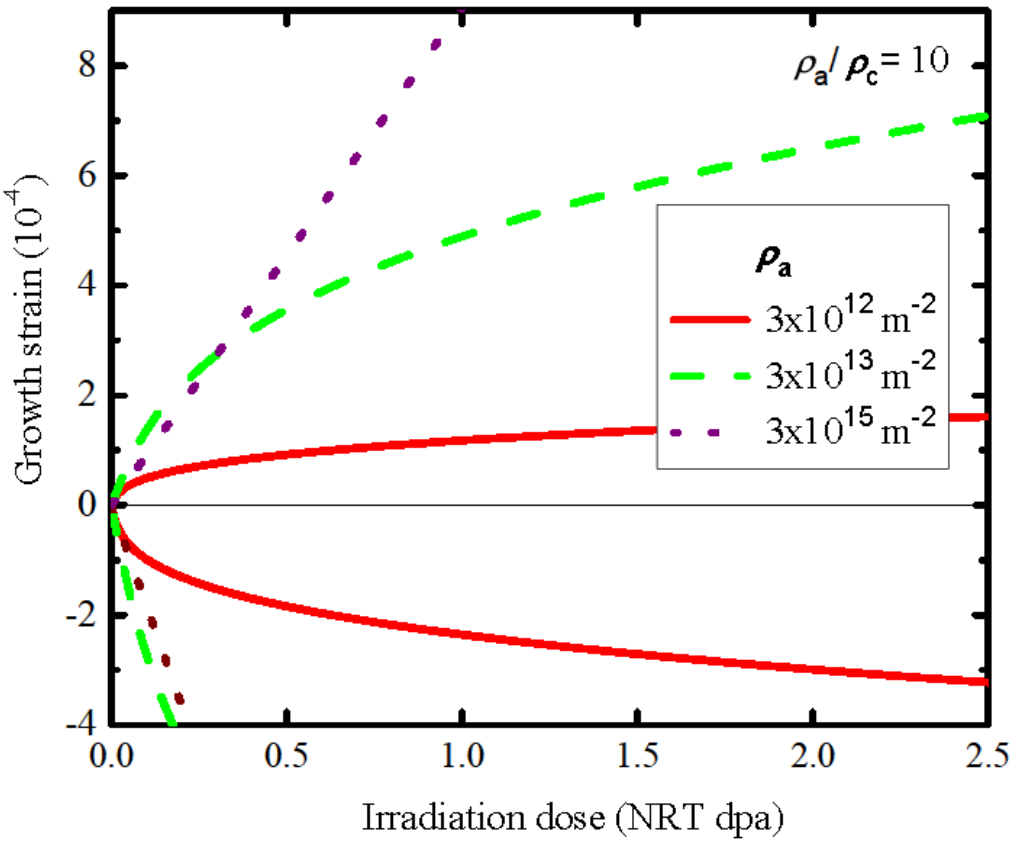
$\rho_a / \rho_c = 10$
ρ_a
$3x10^{12}$ m^{-2}
$3x10^{13}$ m^{-2}
$3x10^{15}$ m^{-2}
Growth strain (10^{-4})
Irradiation dose (NRT dpa)
8
6
4
2
0
-2
-4
0.0
0.5
1.0
1.5
2.0
2.5

Figure 9

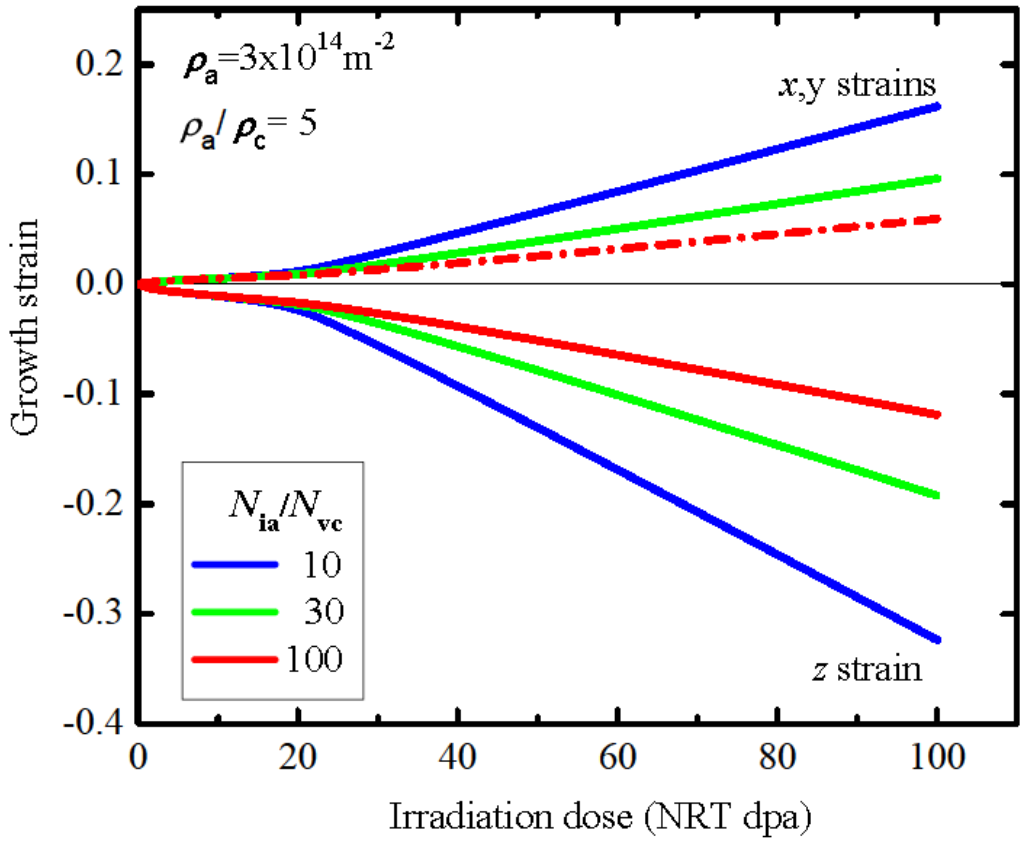
ρ_a=3x10^{14}m^{-2}
ρ_a/ρ_c= 5
x,y strains
z strain
N_{ia}/N_{vc}
10
30
100
Growth strain
Irradiation dose (NRT dpa)
0.2
0.1
0.0
-0.1
-0.2
-0.3
-0.4
0
20
40
60
80
100

Figure 10

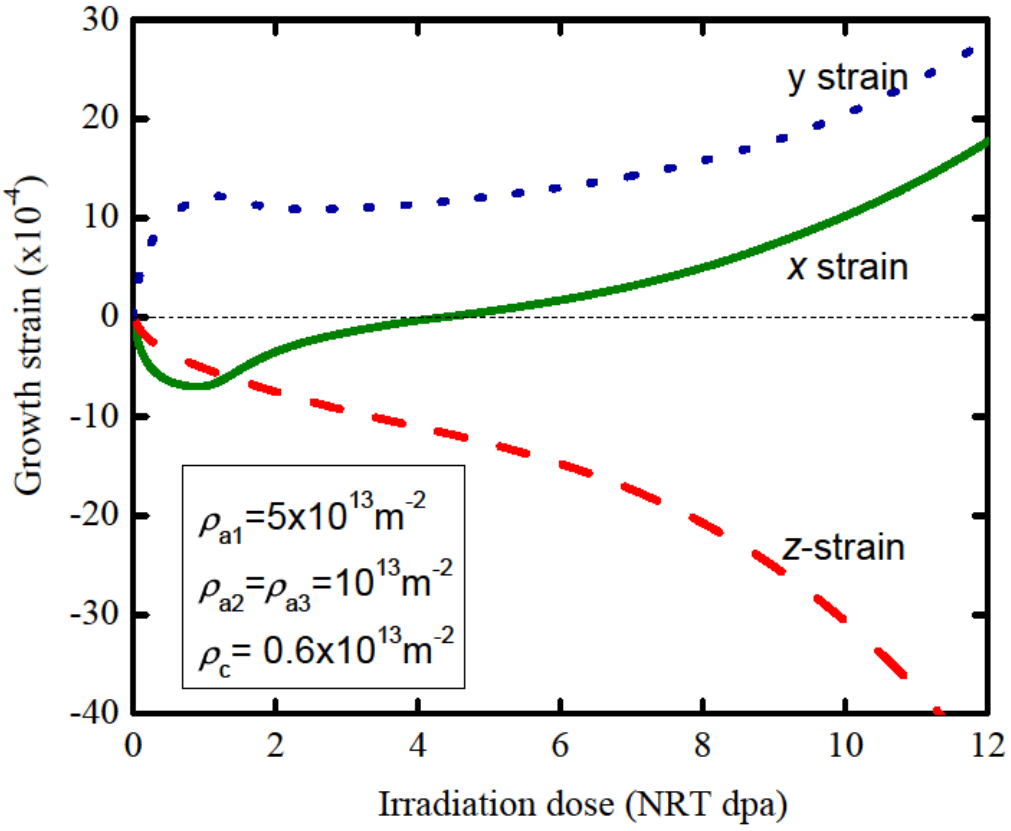
30
20
10
0
-10
-20
-30
-40
0
2
4
6
8
10
12
Growth strain (x10^{-4})
Irradiation dose (NRT dpa)
y strain
x strain
z-strain
ρ_{a1}=5x10^{13}m^{-2}
ρ_{a2}=ρ_{a3}=10^{13}m^{-2}
ρ_c= 0.6x10^{13}m^{-2}